Korean J. of Chem. Eng., 6(2) (1989) 105-111

COMPUTATIONAL SIMULATION OF MELT FLOW IN MAGNETIC CZOCHRALSKI GROWTH PROCESS

Hyung Mann LEE*, Ki-Jun LEE, and Song Yop HAHN**

Department of Chemical Engineering, Seoul National University, Seoul 151-742, Korea

**Department of Electrical Engineering, Seoul National University

(Received 19 April 1988 • accepted 14 October 1988)

Abstract—Melt flow phenomena of magnetic Czochralski processes are simulated numerically. A model is established for the system that can grow a 5 inch diameter single crystal from the melt in a 14 inch diameter cylindrical crucible. Effective conditions to suppress convection adequately are studied by varying rotation rates of the crucible and the crystal for given magnetic fields. When the axial magnetic force is used, the method of co-rotation of the crystal and the crucible is found more effective to suppress meridional circulation than the conventional counter-rotation operation.

INTRODUCTION

One of the most important techniques for growing large-diameter single crystal from the melt is the Czochralski process. A schematic illustration of Czochralski crystal growing process is shown in Fig. 1. Melts of semiconducting material such as silicon are contained in a silica crucible and heated up to approximately 1500°C by external heater, mainly radio frequency heating coils. After appropriate start-up procedures, the growing crystal is slowly pulled upward from the melt. In most applications the crystal is rotated, with the objective of providing a viscous shear layer which tends to isolate the growth interface from the turmoil taking place in the bulk of the melt. In some cases the crucible is also rotated in order to smooth out thermal asymmetries which might arise from irregularities in the heating. The directions of crystal and crucible rotations are usually opposite. To control the contaminant oxygen diffusing from the crucible wall, the exterior of the crucible is surrounded by quartz tubes to make the interior vacuum and sometimes inert gas is also used.

Since 1970, many authors have reported studies on the melt flow during the crystal growth. Some difficulties in experimental observation of the flow behavior have been compensated by the numerical simulations. Kobayashi and Arizumi[1] analyzed computationally flow patterns in the Czochralski crystal growth system using a simple model for various crystal and crucible rotation rates at steady-state conditions. Langlois and Shir[2] obtained the numerical solution of the time-dependent equations governing the flow in a crystal growth crucible. Crochet et al.[3] generated finite element simulations to represent transport phenomena in a Czochralski melt. Later, Langlois[4] suggested that crystals of improved quality might be grown by the Czochralski process if a baffle plate was placed under the crystal face.

The external magnetic field is widely used to suppress the melt flow in the crucible and thereby to obtain high-quality single crystals of silicon in recent years. Both transverse and axial external fields have been applied[5-7]. The quantitative description as to how the imposed field would affect the convection and hence the crystal quality in geometries relevant to the growth of single crystals is rarely reported, with the exception of works by Langlois and Lee [8,9]. Oreper and Szekely [10] found that a magnetic field in the range of kilogauss does significantly suppress the convective flow in the model. Langlois [11,12] surveyed theoretical developments on flow problems related to the Czochralski growth.

Empirical techniques have played an important role in the development of the crystal growth. However, computational methods in recent years made significant contributions to the understanding of the melt flow, as well as to the finding of optimal operating conditions.

In the present study, we have numerically simulated the flow behavior in order to suppress convection, by introducing a model of Czochralski crystal growth process with an axial magnetic field. A model is established for the system that can grow a 5 inch diameter single crystal from the melt in a 14 inch dia-

*Present address; Lucky Central Research Institute, P.O. Box 10, Dae Jeon, Korea

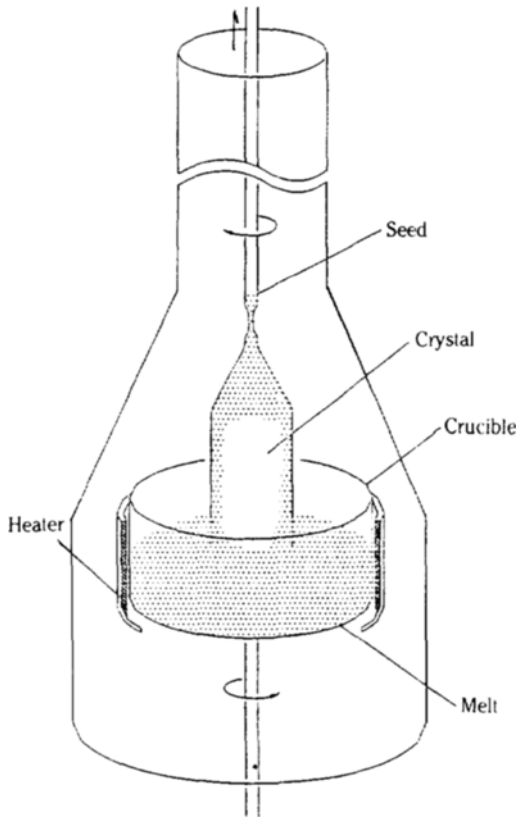

Fig. 1. Schematic illustration of the Czochralski process.

meter cylindrical crucible. The magnetic force effect on the convection is investigated with various rotation rates in a given magnetic force field.

MATHEMATICAL FORMULATION

Theoretical investigations of the convective flow in a Czochralski process employ an idealized configuration in which the top surface is flat and stationary, as shown in Fig. 2. Here R_C and R_S are radii of the crucible and the crystal, respectively, and H is the height of the melt. The rotation velocities Ω_C of the crucible and Ω_S of the crystal are usually in opposite directions. The radial, azimuthal and axial velocity components are denoted by u, v and w, respectively.

Four types of forces act on the Czochralski process with the axial magnetic field: the buoyancy force due to the temperature gradient, the centrifugal force due to the rotation of the crystal and/or the crucible, the thermocapillary force due to the surface tension, and the Lorentz force due to the interaction between the induced current and the externally imposed axial magnetic field.

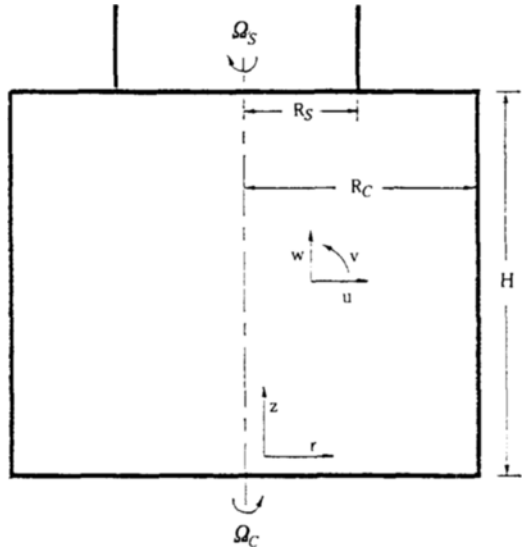

Fig. 2. Geometrical configuration for the bulk-flow idealization.

The presence of the magnetic field and induced current introduces a magnetomotive body force into the Navier-Stokes equation, which then becomes

$$\rho\frac{Dv}{Dt} = -\nabla p - \rho\alpha g\,(T - T_s) + j\times B + \rho\nu\nabla^2 v \quad (1)$$

where ρ,p,α,T_S and ν denote, respectively, the density, the pressure, the volumetric expansion coefficient, the interface temperature and the kinematic viscosity of the melt. And **j** and **B** are the magnetic current density and the magnetic field, respectively. For convenience, a Svanberg vorticity S and a Stokes streamfunction Ψ are introduced such that

$$S = \frac{1}{r}\left(\frac{\partial w}{\partial r} - \frac{\partial u}{\partial z}\right) \quad (2a)$$

$$u = \frac{1}{r}\frac{\partial \Psi}{\partial z} \quad (2b)$$

$$v = -\frac{1}{r}\frac{\partial \Psi}{\partial r}. \quad (2c)$$

The equation for S is obtained by cross-differentiating and substracting the meridional components of equation (1).

$$\frac{\partial S}{\partial t} + \frac{1}{r}\frac{\partial}{\partial r}(ruS) + \frac{\partial}{\partial z}(wS) + \frac{\partial}{\partial z}\left(\frac{\Omega^2}{r^4}\right)$$

$$= \frac{\alpha g}{r}\frac{\partial T}{\partial r} + \frac{\xi}{r^2}\frac{\partial^2 \Psi}{\partial z^2} + \frac{\nu}{r}\frac{\partial}{\partial r}\left[\frac{1}{r}\frac{\partial}{\partial r}(r^2 S)\right] + \nu\frac{\partial^2 S}{\partial z^2} \quad (3)$$

where $\zeta = \sigma B_O^2/\rho$ and $\Omega = rv$ is the swirl (angular momentum per unit mass). σ and B_O are the electrical

conductivity and the magnetic field strength, respectively. Since the azimuthal velocity is not a physically conserved quantity, the equation for the conserved variable Ω is used as follows.

$$\frac{\partial \Omega}{\partial t}+\frac{1}{r}\frac{\partial}{\partial r}(ru\Omega)+\frac{\partial}{\partial z}(w\Omega)$$

$$=-\zeta\frac{\partial \Psi_J}{\partial z}+\frac{\nu}{r}\frac{\partial}{\partial r}\left[r^3\frac{\partial}{\partial r}\left(\frac{\Omega}{r^2}\right)\right]+\nu\frac{\partial^2\Omega}{\partial z^2}. \quad (4)$$

Curves of constant Ψ_J are projections of current-lines onto the meridional planes. The equation for the current function Ψ_J is obtained by cross-differentiating and substracting the components of current density.

$$\frac{\partial}{\partial r}\left(\frac{1}{r}\frac{\partial \Psi_J}{\partial r}\right)+\frac{1}{r}\frac{\partial^2\Psi_J}{\partial z^2}=\frac{1}{r}\frac{\partial \Omega}{\partial z}. \quad (5)$$

The energy equation yields

$$\frac{\partial T}{\partial t}+\frac{1}{r}\frac{\partial}{\partial r}(ruT)+\frac{\partial}{\partial z}(wT)$$

$$=\kappa\left[\frac{1}{r}\frac{\partial}{\partial r}\left(r\frac{\partial T}{\partial r}\right)+\frac{\partial^2 T}{\partial z^2}\right] \quad (6)$$

where κ is the thermal diffusivity of the melt. The governing system of differential equations is completed by combining the three parts of equations (2) to obtain the equation for the streamfunction:

$$\frac{\partial}{\partial r}\left(\frac{1}{r}\frac{\partial \Psi}{\partial r}\right)+\frac{1}{r}\frac{\partial^2\Psi}{\partial z^2}=-rS. \quad (7)$$

Symmetry conditions apply at the axis. On the crucible wall the no-slip velocity condition holds, and the temperature is specified. This temperature need not be the same all over the crucible: in order to get realistic approximation of what occurs in practice, we take the bottom to be slightly less hot than the sidewall. Surface-tension driven flow due to variations in surface tension along the melt surface is caused by the variation in temperature along the surface. According to the relationship that $\mu\partial u/\partial z=\partial\gamma/\partial r$ at the free surface of the melt, the normal derivative of the radial velocity is proportional to the radial derivative of temperature, and the axial velocity vanishes. That is,

$$S=-\frac{1}{r}\frac{\partial u}{\partial z}=-\frac{1}{r}\left(\frac{1}{\mu}\right)\frac{\partial \gamma}{\partial r}=C_{tc}\frac{1}{r}\frac{\partial T}{\partial r} \quad (8)$$

where γ is the surface tension. As a thermal boundary condition, we assume that the free surface loses heat by Stefan-Boltzmann radiation to surroundings that are taken to be at the freezing temperature of the melt.

In summary the conditions obtaining on various segments of the computation region periphery are as follows:

(a) Axis $r=0$

$$u=v=\frac{\partial w}{\partial r}=0,\quad \frac{\partial T}{\partial r}=0$$

(b) Crucible bottom $z=0$

$$u=w=0,\quad v=r\Omega_c,\quad \Omega=\Omega_c r^2,$$

$$S=-\frac{2}{r^2(\Delta z)^2}\Psi(r,\Delta z,t)$$

(c) Crucible wall $r=R_c$

$$u=w=0,\quad v=R_c\Omega_c,\quad \Omega=\Omega_c R_c^2,\quad T=T_c$$

$$S=-\frac{2}{R_c^2(\Delta r)^2}\Psi(R_c-\Delta r,z,t)$$

(d) Interface $z=H$, $r\leq R_s$

$$u=w=0,\quad v=r\Omega_s,\quad \Omega=\Omega_s r^2,\quad T=T_s$$

$$S=-\frac{2}{r^2(\Delta z)^2}\Psi(r,H-\Delta z,t)$$

(e) Free surface $z=H$, $R_s<r<R_c$

$$\frac{\partial v}{\partial z}=w=0,\quad \frac{\partial \Omega}{\partial z}=0,\quad S=C_{tc}\frac{1}{r}\frac{\partial T}{\partial r},$$

$$\left.\frac{\partial T}{\partial t}\right|_{radiation}=-\frac{2\varepsilon^*}{\Delta z}(T^4-T_s^4)$$

where $\varepsilon^*=\frac{\varepsilon\sigma_s}{\rho C_v}$, ε is the surface emissivity, and the parameters ρ, c_v and σ_s are, respectively, the melt density, the melt specific heat and the Stefan-Boltzmann constant.

TECHNIQUE OF SOLUTION

The technique applied at the present study uses a system of grid regions. The simulation was carried out on a 21×30 grid, axially stretched to concentrate grid cells near the top and the bottom [13]. Specifically, there were three uniform regions such that

$z_j=(j-1)\times(0.02\text{cm}),\quad j=1,2,\cdots\cdots6;$

$z_j=3.57\text{cm}+(j-13)\times(0.97\text{cm}),\quad j=13,\cdots\cdots17;$

$z_j=12.0\text{cm}-(30-j)\times(0.02\text{cm}),\quad j=25,\cdots\cdots30.$

In between the above uniform regions, there are regions in which the grid spacing is regulated by the arithmetic progression. The uniform radial grid spacing Δr was chosen as 0.89 cm.

The unsteady equations for the temperature, Swirl and Svanberg vorticity were solved using the "power-law weighted upwind differencing" method. Details of the investigation were reported in ref. [14,15]. This method compensates the diffusion term by the introduction of the correction factor related to the grid Peclet number and has advantages when the convection term is relatively dominant. Although somewhat more complicated than other numerical methods, this method provides an extremely good representation of the exact behavior. To save the computing time, the direct solution method with QL algorithm is used for

the calculation of magnetic current function and streamfunction[16].

RESULTS AND DISCUSSION

A numerical simulation based on the formulation described above was carried out with the parameters shown in Table 1. The crucible of 14 inch(35.56cm) and the crystal of 5 inch(12.7cm) in diameter are chosen. The height of the melt is 12cm. Three fundamental non-dimensional parameters can then be calculated from the above parameters as follows:

Prandtl number $(\nu/\kappa) = 0.024$

Thermal Marangoni number

$$\left(-\frac{\partial\gamma}{\partial T}\frac{(T_c-T_s)R_s}{\rho\nu\kappa}\right)=6.65\times10^4$$

Grashof number

$$\left(\frac{\alpha g R_c^3 (T_c-T_s)}{\nu^2}\right)=7.6\times10^6$$

A numerical investigation is carried out for various cases of magnetic field strength and rotation rates.

Fig. 3 shows the streamlines with a magnetic field of 0.1 tesla for counter-rotation after 50 seconds. The intense circulation of the melt beneath the crystal growing interface is evident with a magnetic field of 0.1 tesla. Following numerical simulations are carried with the magnetic strength of 0.25 tesla since 0.1 tesla seems not enough to suppress the convection in the present study cases. The flow field usually is settled down after about 60 seconds of simulated time, and this was taken as the initial time. Fig. 4 shows the streamlines with a magnetic field of 0.25 tesla. This figure indicates that the convection is suppressed more than the case of 0.1 tesla, and the multicells in the interior represent that the flow becomes weaker gradually. The study of Langlois and Lee[8,9] revealed that

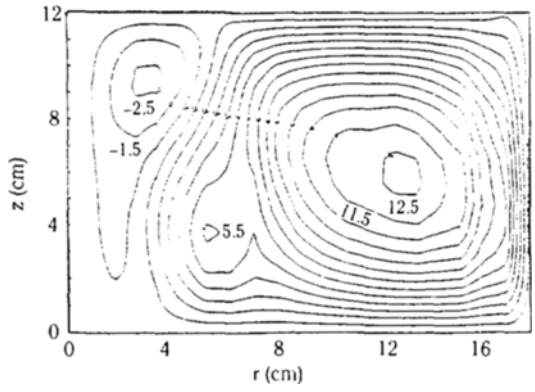

Fig. 3. Streamlines with a magnetic field of 0.1 tesla after 50 seconds.
The contour spacing is 1.0 cm^3/sec.
Counter-rotation; $\Omega_C = 1.57$ radian/sec, $\Omega_S = -2.31$ radian/sec.

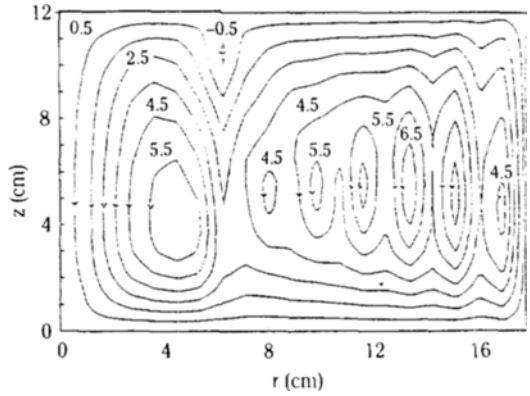

Fig. 4. Streamlines with a magnetic field of 0.25 tesla after 100 seconds.
The contour spacing is 1.0 cm^3/sec.
Counter-rotation; $\Omega_C = 1.57$ radian/sec, $\Omega_S = -2.31$ radian/sec.

Table 1. Physical parameters of silicon

Melt density (ρ): 2.33 g/cm^3
Specific heat capacity (c_v): 0.233 cal/g·K
Thermal diffusivity (κ): 0.125 cm^2/s
Volumetric expansion coefficient (α): 0.0000141/K
Kinematic viscosity (ν): 0.003 cm^3/s
Thermocapillarity coefficient (c_{ic}): 14.9 cm/s·K
Emissivity (ε): 0.318
Crystal temperature (T_S): 1685 K
Crucible temperature (T_C): 1773 K at the wall, decreasing linearly with radius to 1723 K at the center of the bottom
Electrical conductivity (σ): 0.0000125/abohm·cm
Stefan-Boltzmann constant (σ_S): 1.36×10^{-12} cal/cm^2·s·K^4

the higher magnetic field intensities, the greater was the numerical instability near the crucible bottom. By axially stretching the cell space to concentrate still more grid cells close to the top and the bottom, the numerical instability could be overcome.

Transport of heat and trace constituents to the growth interface is influenced by the meridional flow. The volume of melt which circulates in this flow is proportional to the difference between the maximum and minimum values of the Stokes streamfunction, which therefore provides a scalar measure of the convection strength. Fig. 5 plots the history of the quantity for three cases involving counter-rotation of the crystal and the crucible. In each case the crystal rotation rate is -2.31 radian/sec. As shown in the figure, the convection strength at early stages decreases rapidly with

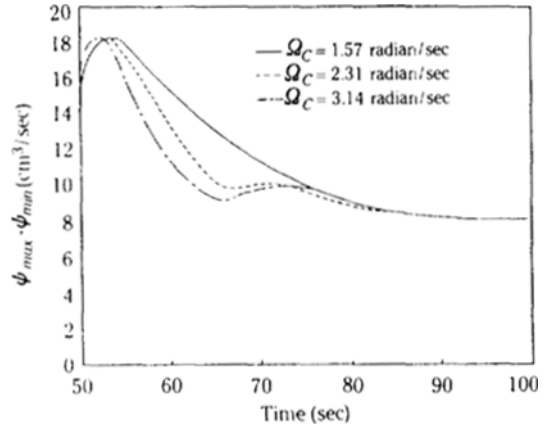

Fig. 5. Effect of the crucible rotation rate on the strength of the meridional circulation (counter-rotation).

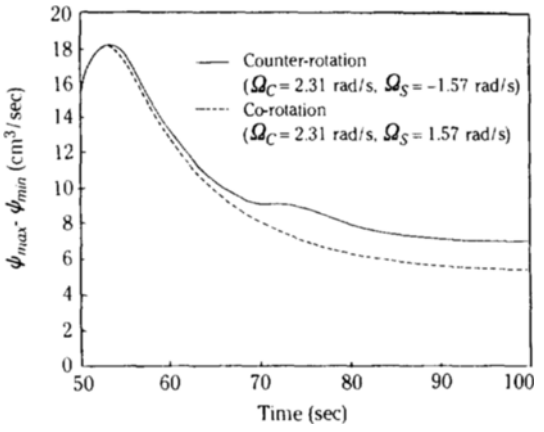

Fig. 7. Effect of the relative direction of rotation on the strength of the meridional circulation.

increasing crucible rotation rate. As time advances, however, the curves coalesce. It thus appears that the crucible rotation rate does not strongly influence the convection suppression in the case of counter-rotation.

For co-rotation, however, a crucible rotation of 2.31 radian/sec is more effective for suppressing the convection than 1.57 radian/sec. This is shown in Fig. 6. The curves are the same whether 2.31 or 1.57 radian/sec is used for the crystal rotation rate, suggesting that the circulation strength does not depend strongly on this quantity.

Thus the relative sense of crystal and crucible rotation is an important factor for the convection strength. Fig. 7 illustrates the dependence. The convection strength with co-rotation is smaller than with the counter-rotation, suggesting that, in conjunction with a magnetic field, co-rotation leads to less melt turmoil than the conventional counter-rotation. A similar result was found for the non-magnetic Czochralski flow in a shallow crucible[4].

Fig. 8 represents the streamlines after 100 seconds for the case of co-rotation. It is found that the melt convection in the case is more suppressed in comparison with the case of counter-rotation. The multicells in the interior region represent the decaying formation of the convection. The temperature distribution for the case of co-rotation is illustrated in Fig. 9. This figure shows that the variations at the neighborhood of the axis is smooth. However the variation is steep in the cases of counter-rotation and no rotation. Temperature gradients near the growth interface exert significant influences on the crystal quality. That is, the temperature distribution beneath the interface indicates the convection strength of the melt.

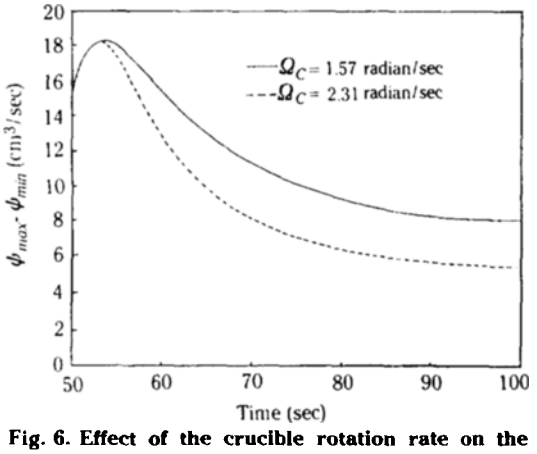

Fig. 6. Effect of the crucible rotation rate on the strength of the meridional circulation(co-rotation).

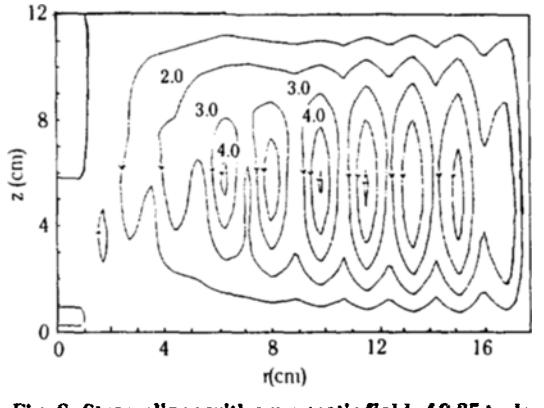

Fig. 8. Streamlines with a magnetic field of 0.25 tesla after 100 seconds.
The contour spacing is 1.0 cm^3/sec.
Co-rotation; Ω_C = 2.31 radian/sec, Ω_S = 1.57 radian/sec.

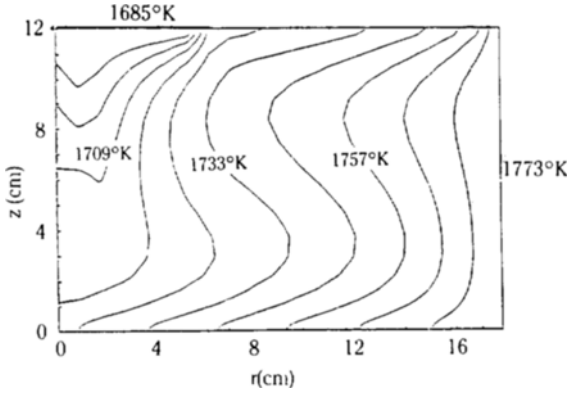

Fig. 9. Temperature distribution with a magnetic field of 0.25 tesla after 100 seconds.
Co-rotation; $\Omega_C = 2.31$ radian/sec, $\Omega_S = 1.57$ radian/sec.

CONCLUSIONS

For a model system that can grow the 5 inch diameter single crystal from the melt in a 14 inch diameter cylindrical crucible, flow problems in the melt have been simulated by the use of numerical methods. When the axial magnetic force is used, the method of co-rotation of the crystal and the crucible is found more effective to suppress meridional circulation than the conventional counter-rotation operation. For counter-rotation, the crucible rotation rate is relatively less sensitive to the convection suppression. However the crucible rotation of 2.31 radian/sec is more effective than that of 1.57 radian/sec to suppress the melt convection in the case of co-rotation. The power-law weighted upwind differencing method is used for the numerical solution of the parabolic equations and found very efficient in computing time-saving. In the present study, numerical simulations have been performed only for the ranges of conventional rotation rates. A further study for wide ranges of rotation rates should be worthwhile to obtain optimum operating conditions.

ACKNOWLEDGEMENT

This research was supported by the grant of the Korea Science and Engineering Foundation.

NOMENCLATURE

$\mathbf{B}$	:	Magnetic field, tesla
B_O	:	Magnetic field strength, tesla
c_{tc}	:	Thermocapillarity coefficient, cm/sec·K
c_v	:	Specific heat capacity, cal/g·K
g	:	Gravitational acceleration, cm/sec^2
H	:	Height of melt, cm
$\mathbf{j}$	:	Magnetic current density, Ampere/cm^2
p	:	Pressure, dyne/cm^2
R_C, R_S	:	Radii of crucible and crystal, respectively, cm
r	:	Distance along r-direction, cm
S	:	Svanberg vorticity, 1/cm·sec
T	:	Temperature, K
T_C, T_S	:	Temperature of crucible and crystal, K
t	:	Time, sec
$\mathbf{v}$	:	Velocity vector, cm/sec
u, v, w	:	Radial, azimuthal and axial velocity components, respectively, cm/sec
z	:	Distance along z-direction, cm

Greek Letters

α	:	Volumetric expansion coefficient, 1/K
γ	:	Surface tension, dynes/cm
ε	:	Emissivity
ζ	:	Coefficient defined in equation(3), $\alpha\ B_o^2/\rho$
κ	:	Thermal diffusivity, cm^2/sec
μ	:	Viscosity, g/cm·sec
ν	:	Kinematic viscosity, cm^2/sec
ρ	:	Density, g/cm^3
σ	:	Electrical conductivity, 1/abohm·cm
σ_S	:	Stefan-Boltzmann constant, cal/cm^2·sec·K^4
Ψ	:	Streamfunction, cm^3/sec
Ψ_J	:	Magnetic current function, cm^3/sec
Ω	:	Swirl, cm^2/sec
Ω_C, Ω_S	:	Rotation rates of crucible and crystal, respectively, radian/sec

REFERENCES

1. Kobayashi, N. and Arizumi, T.: *J. Crystal Growth,* **49,** 419 (1980).
2. Langlois, W.E. and Shir, C.C.: *Comp. Meth. Appl. Mech. Engng,* **12,** 145 (1977).
3. Crochet, M.J., Wouters, P.J., Geyling, F.T., and Jordan, A.S.: *J. Crystal Growth,* **65,** 153 (1983).
4. Langlois, W.E.: *J. Crystal Growth,* **63,** 67 (1983).
5. Hoshikawa, K., Kodha, H., Hirata, H., and Nakanish, H.: *Japan J. Appl. Phys.,* **19,** L33 (1980).
6. Kim, K.M.: *J. Electrochem. Soc.,* **129,** 427 (1982).
7. Hoshikawa, K.: *Japan J. Appl. Phys.,* **21,** L545 (1982).
8. Langlois, W.E. and Lee, K.J.: *IBM Res. Dev.,* **27,** 281 (1983).
9. Langlois, W.E. and Lee, K.J.: *J. Crystal Growth,* **62,** 481 (1983).
10. Oreper, G.M. and Szekely, J.: *J. Crystal Growth,* **64,** 505 (1983).
11. Langlois, W.E.: *Physico. Chem. Hydrodyn.,* **2,**

245 (1981).
12. Langlois, W.E.: *Ann. Rev. Fluid Mech.*, **17,** 191 (1985).
13. Langlois, W.E.: *Comp. Meth. Appl. Mech. Engng,* **25,** 315 (1981).
14. Patankar, S.V.: "Numerical Heat Transfer and Fluid Flow", McGraw-Hill, NY (1980).
15. Lee, H.M.: Ph. D. Dissertation, Seoul National University, Seoul, Korea (1985).
16. Golub, G.H. and Langlois, W.E.: *Comp. Meth. Appl. Mech. Engng,* **19,** 391 (1979).